J. Fluid Mech. (1992), *vol.* 243, *pp.* 679–697
Printed in Great Britain

The resistivity and mobility functions for a model system of two equal-sized proteins in a lipid bilayer

By STUART J. BUSSELL, DONALD L. KOCH AND DANIEL A. HAMMER

School of Chemical Engineering, Cornell University, Ithaca, NY 14853, USA

(Received 31 December 1991 and in revised form 22 March 1992)

We have calculated the mobility and resistivity functions for two equal-sized cylinders moving in a thin viscous sheet surrounded by a lower-viscosity fluid. These functions describe the hydrodynamic interactions between proteins embedded in a lipid bilayer surrounded by an aqueous solution. For a protein of radius a embedded in a biological membrane of thickness h and viscosity μ, a key parameter $\lambda = \mu h/a\mu'$, which characterizes the viscosity ratio between the bilayer and surrounding solution, is $O(100)$. The method of solution for the hydrodynamic interactions differs depending on the separation distance, r, between the cylinders. When $r = O(a)$, the particles are in the near-field regime, and the solution of the Stokes equations is divided between an inner and outer domain based on the asymptotically large value of λ. The inner solution neglects the flow in the lower-viscosity fluid and is solved numerically using a bipolar expansion. The outer solution is based on the fluid flows in all phases, but the cylinders are approximated by net forces. When $r \gg O(a)$, the particles are in the far-field regime, and we use the method of reflections to solve for the hydrodynamic interactions. The uniformly valid approximations, constructed from a combination of the near-field and far-field solutions, agree with the analytic solutions obtained within the lubrication and far-field regimes. Our results show that the hydrodynamic interactions between the cylinders are long range, operating on a lengthscale of $O(\lambda)$. The range of the hydrodynamic interactions is much longer than that of non-hydrodynamic interparticle forces, suggesting that hydrodynamic interactions will be significant determinants of the structure and dynamics of biological membranes.

1. Introduction

The translation and rotation of cylinders in a thin viscous sheet surrounded by lower-viscosity fluid is an appropriate model for the study of the motion of integral membrane proteins in biological and artificial membranes (Saffman 1976; Saffman & Delbruck 1975; Hughes, Pailthorpe & White 1981). This model captures the essential features of the protein–membrane system sketched in figure 1. Many integral membrane proteins have transmembrane domains composed of hydrophobic α-helices with a combined cylindrical radius of a and hydrophillic globular domains which reside in the aqueous phase on either side of the membrane. The α-helical domains of the proteins are stabilized by a large number of hydrogen bonds which resist deformation (Schulz & Schirmer 1979). The membrane, which consists of lipid molecules, has a viscosity μ and a thickness h. The viscosity of the surrounding phase is μ'. Strong thermodynamic forces separate the hydrophobic and hydrophillic domains and restrict the protein and lipid molecules from moving perpendicular to

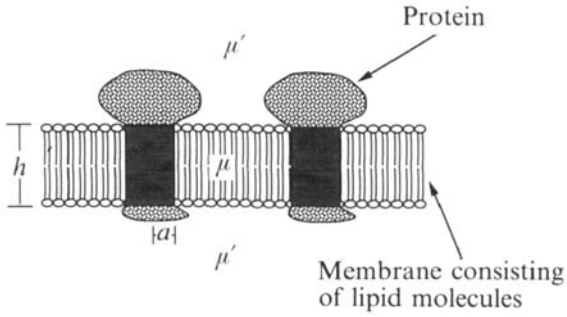

FIGURE 1. Cross-section of a typical biological membrane containing proteins and lipid molecules. The protein molecules have two regimes: a cylindrical core passing through the membrane and globular portions residing in the surrounding fluid.

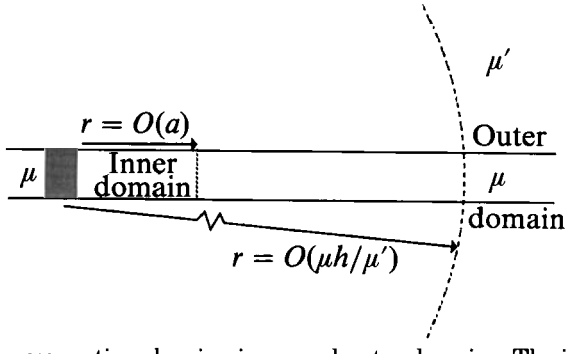

FIGURE 2. Membrane cross-section showing inner and outer domains. The inner domain includes only the membrane, while the outer domain includes all phases. Within the intermediate domain, both the inner and outer solutions are valid.

the plane of the membrane. Furthermore, μ/μ' is typically $O(100)$ for biological systems, and we can neglect the drag of the surrounding phase on the proteins because $\mu' \ll \mu$. The proteins, therefore, can be approximated as cylinders in a thin viscous sheet. The Reynolds number for the disks based on a and μ is $O(10^{-4})$.

This problem was first studied by Saffman (1976) for an isolated cylinder. A review of this work is instructive because many of the results apply to the study of the two-cylinder problem. The rotational problem for an isolated cylinder is straightforward because a convergent solution results when the fluid dynamics in the low-viscosity surrounding phase are ignored. Saffman found that

$$b_r = (4\pi\mu a^2 h)^{-1}, \tag{1}$$

where b_r is the rotational mobility, defined as the steady angular velocity produced by a steady unit torque.

The translational problem, in contrast, is ill-posed when the fluid dynamics of the surrounding phase are ignored because of Stokes paradox. In order to overcome this difficulty, Saffman divided the solution of the problem into an inner and outer regime as illustrated in figure 2. The inner solution, which ignores the surrounding phase and is valid for radial distances $r = O(a)$, is

$$u_r = \cos\theta\left[\frac{F}{8\pi\mu h}(1-\rho^{-2}) + U - \frac{F}{4\pi\mu h}\ln(\rho)\right], \tag{2}$$

where F is the absolute value of the force of the disk on the fluid, $\rho = r/a$, θ is the angle measured from the axis defined by the direction of motion, and U is the

absolute value of the velocity of the cylinder. The inner solution does not satisfy the boundary condition which requires that $u_r \to 0$ as $\rho \to \infty$. At this stage, U is undetermined.

To determine the velocity U, the above inner solution must be matched to an outer solution which satisfies the last boundary condition. In order to calculate the outer solution, Saffman & Delbruck (1975) considered separately the effects of the surrounding phase and the finite extent of the membrane. The drag exerted by the surrounding phase becomes significant at large ρ and causes the velocity field to decay. The drag per unit area exerted by the surrounding phase on a circular area of radius r around the cylinder is $O(\mu' U/r)$. The divergence of the stress within the membrane is $O(\mu h \nabla^2 u) \approx O(\mu h U/r^2)$. These stresses are of the same order at a radial distance $r \approx O(\mu h/\mu')$, which is $O(100a)$ for protein–membrane systems. The finite extent of the membrane becomes important to the translational mobility only if its radius is equal to or smaller than this lengthscale, which is not the case for biological membranes.

The outer solution, valid for $r \gg a$, involves the fluid dynamics in all phases resulting from a point force disturbance in the sheet. The velocity in the membrane obtained from the outer solution is

$$u_r = \frac{F \cos\theta}{4\pi\mu h} \int_0^\infty \frac{J_0(\xi) + J_2(\xi)}{\xi + 2R} \, \mathrm{d}\xi, \tag{3}$$

where J_0 and J_2 are Bessel functions of the first kind of order zero and two, respectively, and $R = r\mu'/(h\mu)$.

The two solutions are matched in the intermediate regime where both solutions are valid, yielding

$$\lim_{\rho \to \infty} (u_r)_{\text{inner}} = \lim_{R \to 0} (u_r)_{\text{outer}}. \tag{4}$$

In the limit as $R \to 0$, (3) becomes

$$u_r = \cos\theta \frac{F}{4\pi\mu h} [-\ln(\rho) + \ln(\lambda) + \tfrac{1}{2} - \gamma], \tag{5}$$

where $\lambda = \rho/R = (\mu h/a\mu')$ and γ is Euler's constant. The criterion which emerges from the match is

$$\frac{U}{F} = \frac{1}{4\pi\mu h} [\ln(\lambda) - \gamma]. \tag{6}$$

The match between the two solutions depends upon λ, and the error in the outer solution introduced by the point-force approximation is $O(\lambda^{-2})$. The solution for a single particle contains no dipole term, which is $O(\rho^{-1})$ in the inner solution, so this error estimate is based on the neglected quadrupole term, $O(\rho^{-2})$, evaluated at $r = \mu h/\mu'$. The right-hand side of (6) is the translational mobility, b_t, which is defined as the velocity produced by a unit force.

The results derived by Saffman are successful in predicting both D_t and D_r, the translational and rotational diffusion coefficients, respectively, at low protein concentration (Peters & Cherry 1982; Vaz, Goodsaid-Zalduondo & Jacobson 1984). On the other hand, the Saffman results fail to predict D_t and D_r as protein concentration increases because protein–protein interactions become important (Vaz *et al.* 1984).

Previous treatments of protein diffusion at higher concentrations have included potential energy interactions and/or excluded volume effects while neglecting

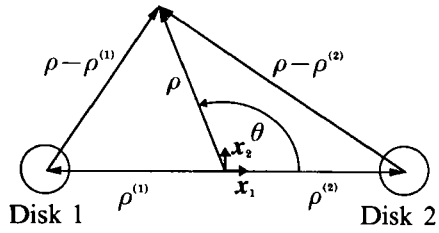

FIGURE 3. Schematic detailing the coordinate system for the calculation of the inner solution. The origin is located midway between the two disks, and both cylindrical and Cartesian coordinates are used.

hydrodynamic interactions (Abney, Scalettar & Owicki 1989; Pink, Laidlaw & Chisholm 1986; Saxton 1987). They have been successful at predicting some of the experimental trends, but they fail to capture all of the physics of the problem. These methods predict qualitatively how D_t decreases with protein area fraction but fail to quantitatively match the data (Saxton 1987). The large lengthscale for the velocity disturbance calculated for an isolated particle suggests hydrodynamic interactions between proteins will be important even at low concentrations and may help account for the discrepancy between experimental measurements and current theoretical predictions.

The objective of this paper is to determine the hydrodynamic interactions which exist between two equal-sized cylinders in a thin viscous sheet surrounded by a lower-viscosity fluid as a model system for elucidating hydrodynamic interactions between proteins in membranes. These interactions are succinctly tabulated by the resistivity and mobility matrices, represented as $\boldsymbol{R}$ and $\boldsymbol{M}$, respectively (Brenner & O'Neill 1972; Kim & Karrila 1991). The matrices are the linear relations between the rigid-body motions of the cylinders and the forces and torques exerted by the cylinders on the fluid. The linearity of these relations is valid because the fluid dynamics are governed by Stokes equations in both the membrane and the surrounding fluid.

The elements of the mobility matrix relate the motions of the cylinders to the forces and torques which they apply to the fluids. This relationship is summarized below,

$$\begin{bmatrix} U_1^{(1)} \\ U_2^{(1)} \\ a\omega^{(1)} \\ U_1^{(2)} \\ U_2^{(2)} \\ a\omega^{(2)} \end{bmatrix} = \boldsymbol{M} \begin{bmatrix} F_1^{(1)}/\mu h \\ F_2^{(1)}/\mu h \\ L^{(1)}/\mu h a \\ F_1^{(2)}/\mu h \\ F_2^{(2)}/\mu h \\ L^{(2)}/\mu h a \end{bmatrix}, \tag{7}$$

where we have used the coordinate conventions detailed in figure 3, superscripts identify the cylinder number, subscripts identify direction, and L is torque. The coordinate vectors are scaled with a, and the gap width, ϵ, is equal to $|\rho^{(1)}-\rho^{(2)}|-2$. Because the proteins are restricted to motions in the plane of the membrane, their torque and angular velocity are represented by a single scalar component in the x_3-direction. The resistivity matrix, the inverse of $\boldsymbol{M}$, relates the force and torque exerted by the cylinders on the fluids to the cylinder motions.

Both $\boldsymbol{M}$ and $\boldsymbol{R}$ are 6×6 matrices with 36 components, but the reciprocal theorem of Lorentz (1907) and the symmetry of the problem reduce the number of independent scalars in both matrices. The reciprocal theorem can be used to show

that $\boldsymbol{M}$ and $\boldsymbol{R}$ are symmetric, reducing the number of independent scalars from 36 to 21. The symmetry of the two-cylinder geometry further reduces the number of independent scalars in $\boldsymbol{M}$ and $\boldsymbol{R}$ to 8. Thus, $\boldsymbol{M}$ takes the form

$$\boldsymbol{M}=\begin{bmatrix} a & 0 & 0 & b & 0 & 0 \\ 0 & c & d & 0 & e & f \\ 0 & d & g & 0 & -f & h \\ b & 0 & 0 & a & 0 & 0 \\ 0 & e & -f & 0 & c & -d \\ 0 & f & h & 0 & -d & g \end{bmatrix}. \tag{8}$$

Conversion between $\boldsymbol{M}$ and $\boldsymbol{R}$ is straightforward because each is a scalar matrix, and $\boldsymbol{M}=\boldsymbol{R}^{-1}$. The resistivity matrix is

$$\boldsymbol{R}=\begin{bmatrix} A & 0 & 0 & B & 0 & 0 \\ 0 & C & D & 0 & E & F \\ 0 & D & G & 0 & -F & H \\ B & 0 & 0 & A & 0 & 0 \\ 0 & E & -F & 0 & C & -D \\ 0 & F & H & 0 & -D & G \end{bmatrix}. \tag{9}$$

The relationships between the components of $\boldsymbol{R}$ and $\boldsymbol{M}$ are given in Appendix A.

In order to solve for the components of $\boldsymbol{R}$ and $\boldsymbol{M}$ when ϵ is $O(1)$, we use the same approximations as Saffman (1976) to divide the problem into an inner and outer solution. When $\epsilon \gg 1$, we use the method of reflections. We combine these solutions into a uniformly valid approximation which conforms to the lubrication and far-field asymptotes, each of which is analytically accessible.

2. Method

In this section we present the method for calculating the hydrodynamic interactions between two equal cylinders immersed in a thin viscous sheet surrounded by lower viscosity fluid. The Reynolds number is small so that the fluid motion is governed by Stokes equations. There are two regimes, a near-field and a far-field regime, for the solution based on $|\rho^{(1)}-\rho^{(2)}|$, the separation distance between the two particles. When $|\rho^{(1)}-\rho^{(2)}| = O(a)$, the particles are in the near-field regime, and the hydrodynamic interactions between the particles are both strong and dominated by the membrane. For this case, the problem of determining the fluid velocity is divided into inner and outer domains based on the large viscosity ratio between the thin sheet and the surrounding fluid. The inner problem satisfies the boundary conditions on the cylinders and ignores the hydrodynamics in the surrounding fluid. It is a two-dimensional problem and is solved using a twin-pole expansion technique (Sangani & Yao 1988). The outer problem satisfies the boundary conditions at infinity and approximates the cylinders as a single point force. Its solution is identical to the one derived by Saffman (1976) for the one-particle problem. The two solutions are matched in order to obtain the final result.

When $|\rho^{(1)}-\rho^{(2)}| \gg O(a)$, the particles are in the far-field regime, and the hydrodynamic interactions are logarithmically weak. At large separations, the interactions between the particle motions are no longer dominated by the membrane. Rather, they are controlled by the fluid dynamics in all phases. They are calculated using the method of reflections (Kim & Karrila 1991) based on the outer solution.

2.1. *Near-field solution, inner problem*

We solve the inner problem with a numerical technique which expands the fluid velocity in the fundamental solutions for Stokes flow in two-dimensions (Sangani & Yao 1988). The velocity field is a function of the fundamental solution, and all its derivatives, expanded about the centre of each disk. However, our problem has a different fundamental solution than the problem addressed by Sangani & Yao. They were interested in N particles with periodic boundary conditions, while we are interested in a non-periodic solution with two cylinders.

The velocity within the inner domain of the membrane satisfies Stokes equations. We solve these equations using dimensionless variables (indicated with overbars). Distances are scaled with a. We have arbitrarily chosen to scale the equations with force or torque. Taking Z to be a general driver, either F or L/a, $\boldsymbol{u} = Z/(h\mu)\,\bar{\boldsymbol{u}}$ and $p = Z/(ha)\,\bar{p}$, where $\boldsymbol{u}$ is the dimensional fluid velocity and p is the pressure. Thus, Stokes equations become

$$\nabla^2\bar{\boldsymbol{u}} = \nabla\bar{p}, \tag{10}$$

and,

$$\nabla\cdot\bar{\boldsymbol{u}} = 0. \tag{11}$$

The governing equations are conveniently written in terms of the dimensionless stream function, Ψ, and vorticity ω, and become

$$\nabla^2\omega = 0, \quad \nabla^2\Psi = -\omega. \tag{12a, b}$$

We expand ω in the fundamental solution of Laplace's equation,

$$G_1 = \frac{1}{2\pi}\ln(\rho-\rho^{(n)}), \tag{13}$$

where G_1 satisfies,

$$\nabla^2 G_1 = \delta(\rho-\rho^{(n)}). \tag{14}$$

The vorticity takes the form

$$\omega = -\sum_{n=1}^{2}\sum_{l=1}^{\infty}\sum_{m=0}^{1}\left[A_{lm}^{(n)}\frac{\partial^l}{(\partial x_1)^{l-m}\,\partial x_2^m}G_1(\rho-\rho^{(n)})\right]. \tag{15}$$

The stream function, Ψ, is expressed as a sum of the homogeneous and particular solutions to (12b). The homogeneous solution is similar to the expression for ω, and the particular solution is expanded in terms of G_2. The function G_2 replaces S_2 used by Sangani & Yao and satisfies the following equation:

$$\nabla^2 G_2 = -G_1. \tag{16}$$

The expression for G_2 is,

$$G_2 = \frac{-\rho^2}{2\pi}[\ln(\rho-\rho^{(n)})-1]. \tag{17}$$

Thus,

$$\Psi = c_1 x_2 - c_2 x_1 + \sum_{n=1}^{2}\left\{B_{00}^{(n)}G_1(\rho-\rho^{(n)}) + \left[\sum_{l=1}^{\infty}\sum_{m=0}^{1}\frac{\partial^l}{(\partial x_1)^{l-m}\,\partial x_2^m}[A_{lm}^{(n)}G_2(\rho-\rho^{(n)}) + B_{lm}^{(n)}G_1(\rho-\rho^{(n)})]\right]\right\}, \tag{18}$$

where the coefficients, $A_{lm}^{(n)}$ and $B_{lm}^{(n)}$, are determined by the boundary conditions, and c_1 and c_2 are determined by matching to the outer solution. In Appendix B, we give concise expressions for the derivatives of G_1 and G_2.

The two components of the fluid velocity, $\bar{u}_1$ and $\bar{u}_2$, result from differentiating Ψ,

$$\left.\begin{aligned}\bar{u}_1 = c_1 + \sum_{n=1}^{2}\Bigg[B_{00}^{(n)}\frac{\partial G_1(\rho-\rho^{(n)})}{\partial x_2} + \sum_{l=1}^{\infty}\sum_{m=0}^{1}\frac{\partial^{l+1}}{(\partial x_1)^{l-m}\,\partial x_2^{m+1}}\left[A_{lm}^{(n)}\,G_2(\rho-\rho^{(n)})\right.\\ \left.+B_{lm}^{(n)}\,G_1(\rho-\rho^{(n)})\right]\Bigg]\end{aligned}\right\}$$

and

$$\left.\begin{aligned}\bar{u}_2 = c_2 - \sum_{n=1}^{2}\Bigg[B_{00}^{(n)}\frac{\partial G_1(\rho-\rho^{(n)})}{\partial x_1} + \sum_{l=1}^{\infty}\sum_{m=0}^{1}\frac{\partial^{l+1}}{(\partial x_1)^{l-m+1}\,\partial x_2^{m}}\left[A_{lm}^{(n)}\,G_2(\rho-\rho^{(n)})\right.\\ \left.+B_{lm}^{(n)}\,G_1(\rho-\rho^{(n)})\right]\Bigg].\end{aligned}\right\} \tag{19}$$

Substituting these results into Stokes equation, (10), we find $\bar{p}$,

$$\bar{p} = \sum_{n=1}^{2}\left\{\left[A_{11}^{(n)}\frac{\partial}{\partial x_1} - A_{10}^{(n)}\frac{\partial}{\partial x_2}\right]G_1(\rho-\rho^{(n)}) + \left[\sum_{l=2}^{\infty}\sum_{m=0}^{1}A_{10}^{(n)}\frac{\partial^l G_1(\rho-\rho^{(n)})}{(\partial x_1)^{l-m-1}\,\partial x_2^{m+1}}\right]\right\}. \tag{20}$$

The boundary conditions are easiest to apply using the resistivity formulation because the disk velocities are given by integral equations over the surfaces of the disks. The no-slip boundary conditions are

$$\int_0^{2\pi}\bar{\boldsymbol{u}}(\rho)\,\mathrm{e}^{\mathrm{i}l\theta}\,\mathrm{d}\theta = C_l \quad \text{on} \quad \partial D^{(n)}, \tag{21}$$

where $\partial D^{(n)}$ is the surface of disk n. The boundary condition, C_l, equals the linear velocity for $l=0$, equals $\frac{1}{2}(a\omega)(1-i)$ for $l=1$, and equals zero for $l\geqslant 2$. In the integration of (21), the series for $\bar{\boldsymbol{u}}(\rho)$ is truncated at $l=L_{\max}$ in order to obtain a finite system of equations. This results in $2(4L_{\max}+2)$ equations in $2(4L_{\max}+1)$ unknowns. However, of the four equations for $l=1$, only three are linearly independent, and one can be discarded. This is a consequence of the stream-function formulation which automatically satisfies the continuity equation. The value of $L_{\max}$ is systematically increased until the desired accuracy is attained.

The integral in (21) is evaluated in two parts. The first part involves terms expanded around disk n, and the second part involves terms expanded around the other disk. The terms in the latter integral must be transformed into multipoles centred at disk n. In Appendix C, we restate the theorems governing this transformation (Sangani & Yao 1988). Finally, orthogonal properties of sine and cosine are used to evaluate the coefficients, $A_{lm}^{(n)}$ and $B_{lm}^{(n)}$.

The forces and torques exerted by the disks on the fluid are

$$\bar{F}_i^{(n)} = \frac{F_i^{(n)}}{Z} = -\int_{\partial V^{(n)}}\frac{\partial \bar{T}_{ij}}{\partial x_i}\,\mathrm{d}V, \quad \bar{L}^{(n)} = \frac{L^{(n)}}{aZ} = \epsilon_{3jk}\int_{\partial V^{(n)}}\frac{\partial \bar{T}_{jl}}{\partial x_l}\,x_k\,\mathrm{d}V, \tag{22}$$

where $\partial V^{(n)}$ is the volume of disk n. The dimensionless stress tensor is

$$\bar{T}_{ij} = -\bar{p}\,\delta_{ij} + \frac{\partial \bar{u}_i}{\partial x_j} + \frac{\partial \bar{u}_j}{\partial x_i}, \tag{23}$$

and the derivatives of the stress tensor are

$$\frac{\partial \bar{T}_{1j}}{\partial x_j} = \sum_{n=1}^{2}\left\{B_{00}^{(n)}\frac{\partial \delta(\rho-\rho^{(n)})}{\partial x_2} - A_{11}^{(n)}\,\delta(\rho-\rho^{(n)}) + \left[\sum_{l=1}^{\infty}\sum_{m=0}^{1}B_{lm}^{(n)}\frac{\partial^{l+1}\delta(\rho-\rho^{(n)})}{(\partial x_1)^{l-m}\,\partial x_2^{m+1}}\right]\right\} \tag{24a}$$

and

$$\frac{\partial \bar{T}_{2j}}{\partial x_j} = \sum_{n=1}^{2} \left\{ -B_{00}^{(n)} \frac{\partial \delta(\rho-\rho^{(n)})}{\partial x_1} + A_{10}^{(n)} \delta(\rho-\rho^{(n)}) + \left[\sum_{l=2}^{\infty} \sum_{m=0}^{1} A_{lm}^{(n)} \frac{\partial^{l-1}\delta(\rho-\rho^{(n)})}{(\partial x_1)^{l-m-1}\partial x_2^m} \right] - \left[\sum_{l=1}^{\infty} \sum_{m=0}^{1} B_{lm}^{(n)} \frac{\partial^{l+1}\delta(\rho-\rho^{(n)})}{(\partial x_1)^{l-m+1}\partial x_2^m} \right] \right\}. \quad (24b)$$

Substituting (24) into (22), we find

$$\bar{F}_1^{(n)} = A_{11}^{(n)}, \quad \bar{F}_2^{(n)} = -A_{10}^{(n)}, \quad \bar{L}^{(n)} = -2B_{00}^{(n)} + A_{20}^{(n)}. \quad (25)$$

Results for $\bar{u}_1$ and $\bar{u}_2$, at this point, are only known to within the constant terms, c_1 and c_2, except for cases without a net force, for which both constants equal zero. For cases involving a net force, the constants are determined by matching the inner solution to the outer solution.

2.2. *Near-field solution, outer problem and matching*

The outer problem for two cylinders separated by an $O(a)$ distance is identical to that for a single cylinder (Saffman 1976) because, in both cases, only the net force is important. Therefore, the outer solution is given by (3).

Because the outer solution is identical for the single- and dual-cylinder situations, the matching criteria to determine c_1 and c_2 are analogous to the one used for a single cylinder, provided that we do the matching using the mobility formulation. If we matched the two solutions using the resistivity formulation, however, the cylinder's velocities would be both an input, as boundary conditions, and a output in the matching procedure. This would necessitate an extra iteration to fix some of the components of $\boldsymbol{R}$. Thus, the matching is easiest to apply to the elements of the mobility tensor because the forces and torques, the boundary conditions in this formulation, are independent of the matching procedure. The matching, therefore, simply fixes the values of $\bar{u}_1$ and $\bar{u}_2$. We find

$$c_n = \frac{\bar{F}_{(n)}}{4\pi}[\ln(\lambda) - \gamma], \quad (26)$$

where $\bar{F}_{(n)}$ is the net force in the $\boldsymbol{x}_n$-direction, and $n = 1$ or 2. The error introduced by replacing the cylinders with a net force in order to calculate the outer solution is $O(\lambda^{-1})$, in contrast to the $O(\lambda^{-2})$ error for the single-particle problem, because the dipole term is now the lowest neglected term which contributes to the solution. In the results section, we vary λ from 100 to 750, with 250 being a typical value found in biological systems.

2.3. *Far-field solution*

The method just described applies well for gap widths, ϵ, of $O(1)$ and is therefore a near-field solution. As the value of ϵ becomes $O(\lambda)$, however, neglecting the fluid dynamics in the surrounding phase in the calculation of the inner solution introduces significant errors. We calculate a far-field solution by again exploiting the large value of λ. We use the method of reflections in the same way that it is applied to two spheres separated by a large distance (Kim & Karrila 1991). Because λ is $O(100)$, we need only include the first reflection in the calculation.

We calculate the far-field results using the mobility formulation, and the reasons for this choice will become clear later. The zeroth-order solution for the cylinder

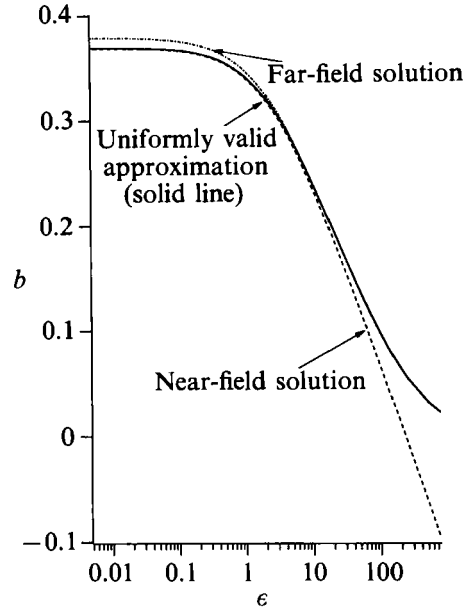

FIGURE 4. Comparison of the near-field, far-field, and uniformly valid approximations for the mobility component b with $\lambda = 250$.

velocities, ${}^{(0)}U$, is given by the independent application of (6) to each cylinder and is $O(\ln \lambda)$. The mutual presence of the cylinders, however, alters their velocities through the transmission of velocity disturbances. The velocity disturbances are calculated using the outer solution for a single cylinder, (3), since the cylinders are at a large separation distance. The integral in (3) is evaluated numerically. At ϵ of $O(\lambda)$ and zeroth order, the velocity disturbance, ${}^{(0)}u|_{\epsilon=\lambda}$, is $O(1)$. The first reflection evaluates the effect of the zeroth-order velocity disturbances on each cylinder. The first-order disturbance of the cylinder velocities, ${}^{(1)}U$, is ${}^{(0)}u|_{\epsilon=\lambda}$, which we already know is $O(1)$. This is the point at which we truncate our calculation of the far-field solution. However, we continue the procedure in order to estimate the errors introduced by neglecting the higher-order terms. The stresslet, S, is the lowest pole affected by the velocity disturbances because the force and torque on each disk are set by the boundary conditions. The first-order stresslet, proportional to $\nabla {}^{(0)}u|_{\epsilon=\lambda}$, is $O(\lambda^{-1})$, and it creates a first-order velocity disturbance equal to ${}^{(1)}S[(\epsilon+2)^{-1}]|_{\epsilon=\lambda}$ which is $O(\lambda^{-2})$. The second-order disturbance of the cylinder velocities, ${}^{(2)}U$, is ${}^{(1)}u|_{\epsilon=\lambda}$ which is $O(\lambda^{-2})$. In a like manner, we find that each successive cylinder velocity disturbance decreases by $O(\lambda^{-2})$ relative to the previous one.

For comparison we have also estimated the strength of the reflections using the resistivity formulation. The zeroth-order solution for the cylinder forces, ${}^{(0)}F$, is, as above, given by the independent application of (6) to each cylinder and is $O(\ln^{-1}\lambda)$. At ϵ of $O(\lambda)$ and zeroth order, the velocity disturbance, ${}^{(0)}u|_{\epsilon=\lambda}$, is also $O(\ln^{-1}\lambda)$. The first-order disturbance of the cylinder forces, ${}^{(1)}F$, is $O(\ln\lambda)$ smaller than ${}^{(0)}u|_{\epsilon=\lambda}$ or $O(\ln^{-2}\lambda)$. Continuing the procedure, each successive cylinder force disturbance decreases by $O(\ln^{-1}\lambda)$ relative to the previous one. The neglect of second- and higher-order reflections in the resistivity formulation introduces $O(\ln^{-1}\lambda)$ relative errors instead of the $O(\lambda^{-2})$ errors in the mobility formulation. Therefore, the mobility formulation is more precise for the calculation of the far-field solution. This is the

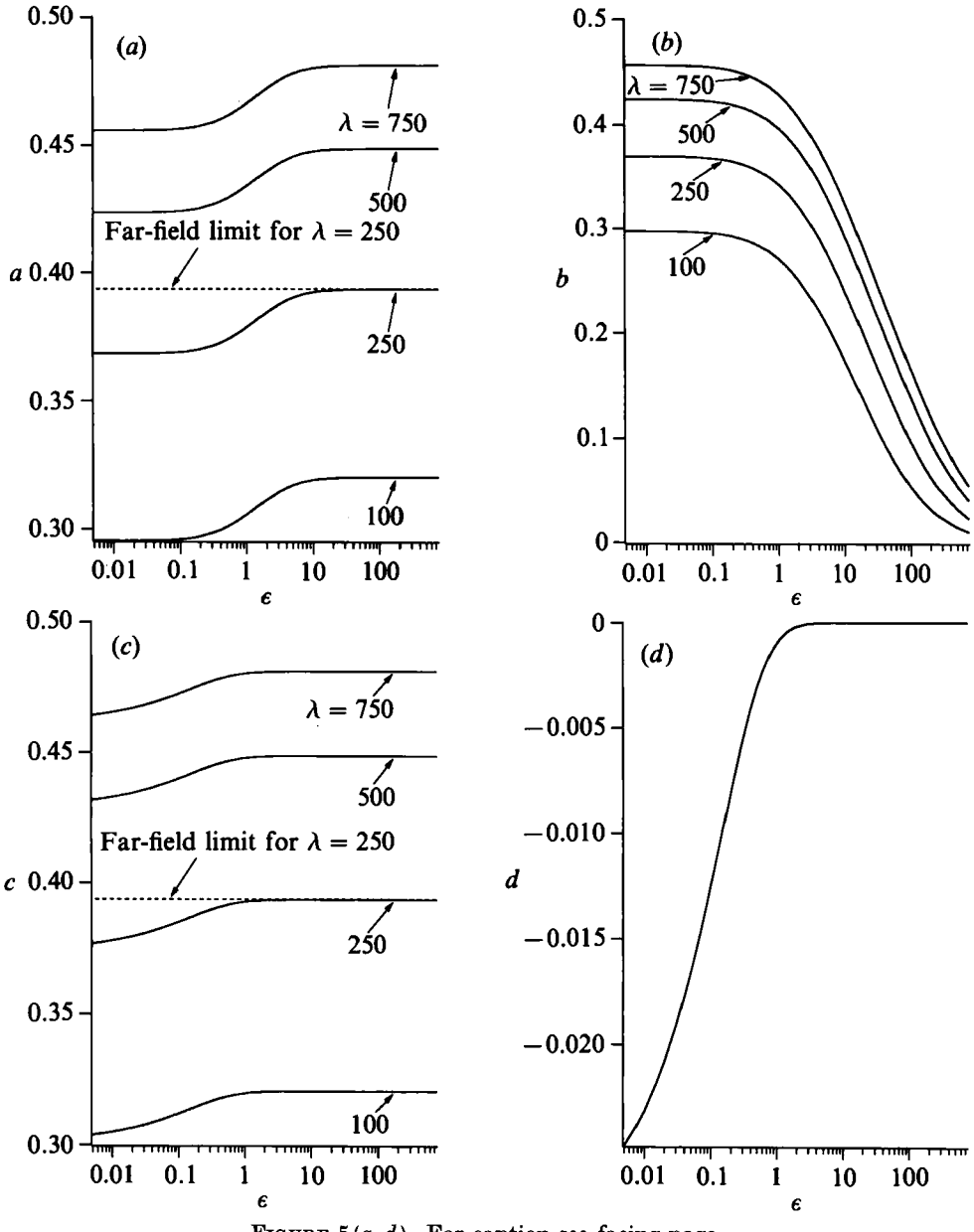

FIGURE 5(*a–d*). For caption see facing page.

same conclusion as found for normal Stokes flow. For this reason, Stokesian dynamic simulations employ the mobility formulation to calculate hydrodynamic interactions between widely separated particles (Brady & Bossis 1988).

3. Results

In this section we present the results for the hydrodynamic interactions at all separation distances between two cylinders in a thin viscous sheet. We demonstrate that our results smoothly approach both the far-field and lubrication solutions. The

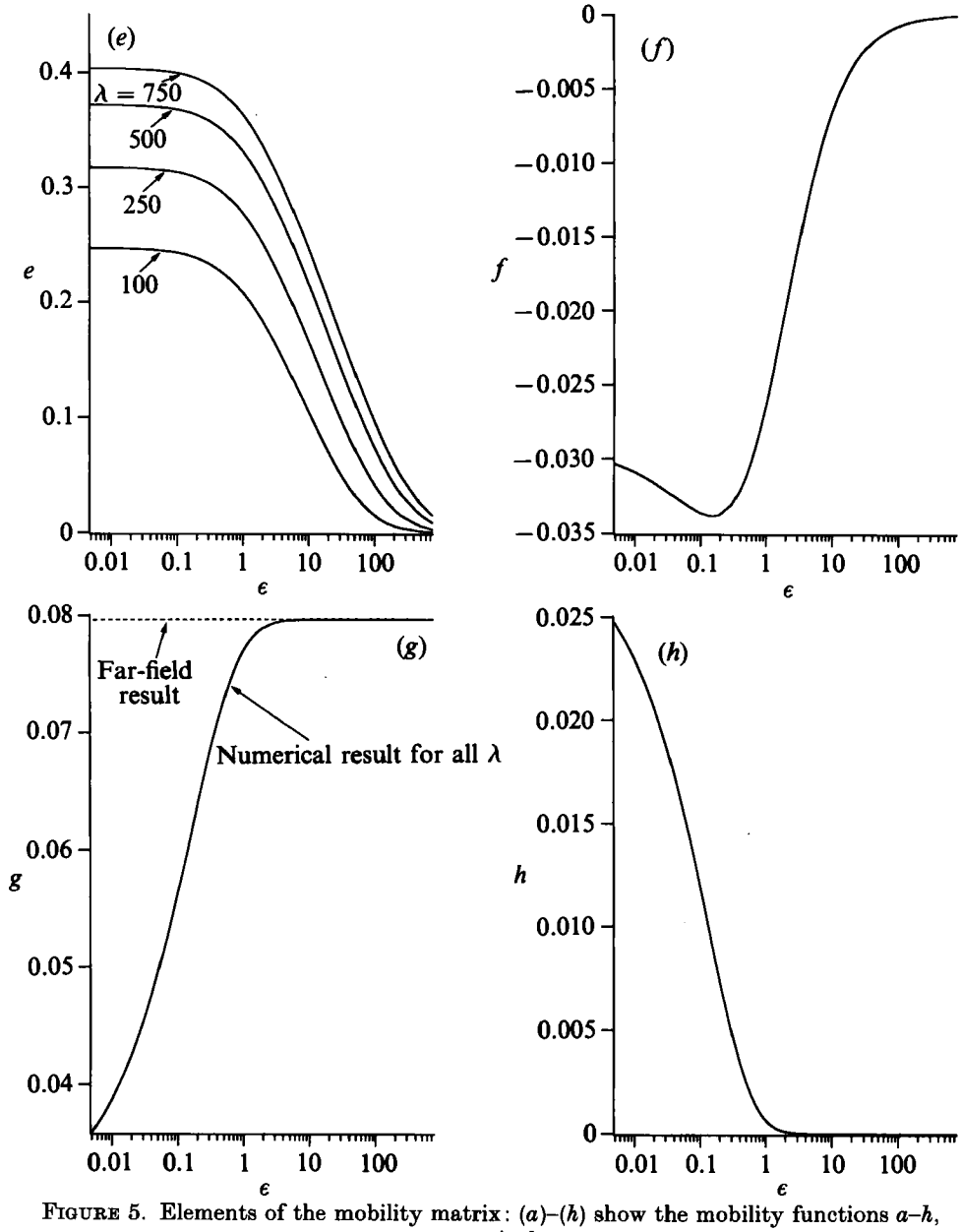

FIGURE 5. Elements of the mobility matrix: (*a*)–(*h*) show the mobility functions *a*–*h*, respectively.

lubrication terms are most obvious in the resistivity results because they are asymptotically large in that formulation.

We evaluated the inner solution numerically and chose $L_{\max}$ to satisfy a 0.001 relative convergence criterion for the forces and torques. The raw data from these calculations are available elsewhere (Bussell 1992). When ρ is large, convergence occurs with only one or two terms. However, when ρ is small, convergence requires many more: for example, 87 terms were used at $\epsilon \approx 0.0075$ to ensure convergence for all components.

The mobility matrix results for various values of λ are given in figures 4 and 5.

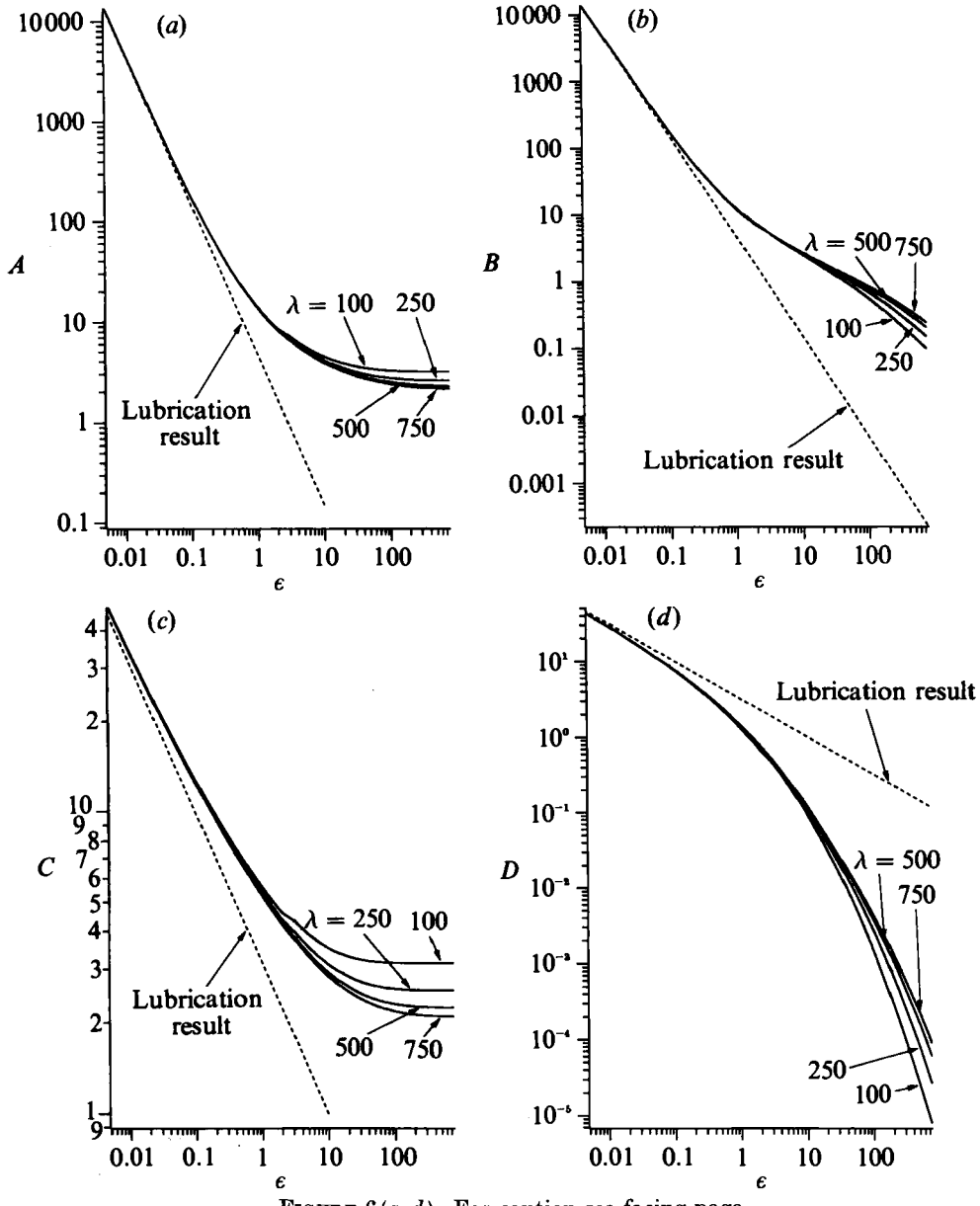

FIGURE 6(*a–d*). For caption see facing page.

Figure 4 demonstrates that the uniformly valid approximation smoothly bridges the regime between the near-field and far-field solutions for component b. The uniformly valid approximations result from the addition of the numerical near-field solution and the analytical far-field solution and subsequent subtraction of the common limit. Figure 5 contains the uniformly valid approximations for the components of the mobility matrix. Some components are independent of λ because they do not depend on the matching operation. The far-field solutions appear in the graphs when they are non-zero.

The resistivity results for various λ appear in figure 6. We calculate the components of $\boldsymbol{R}$ from the results for $\boldsymbol{M}$ by using the relationships in Appendix A.

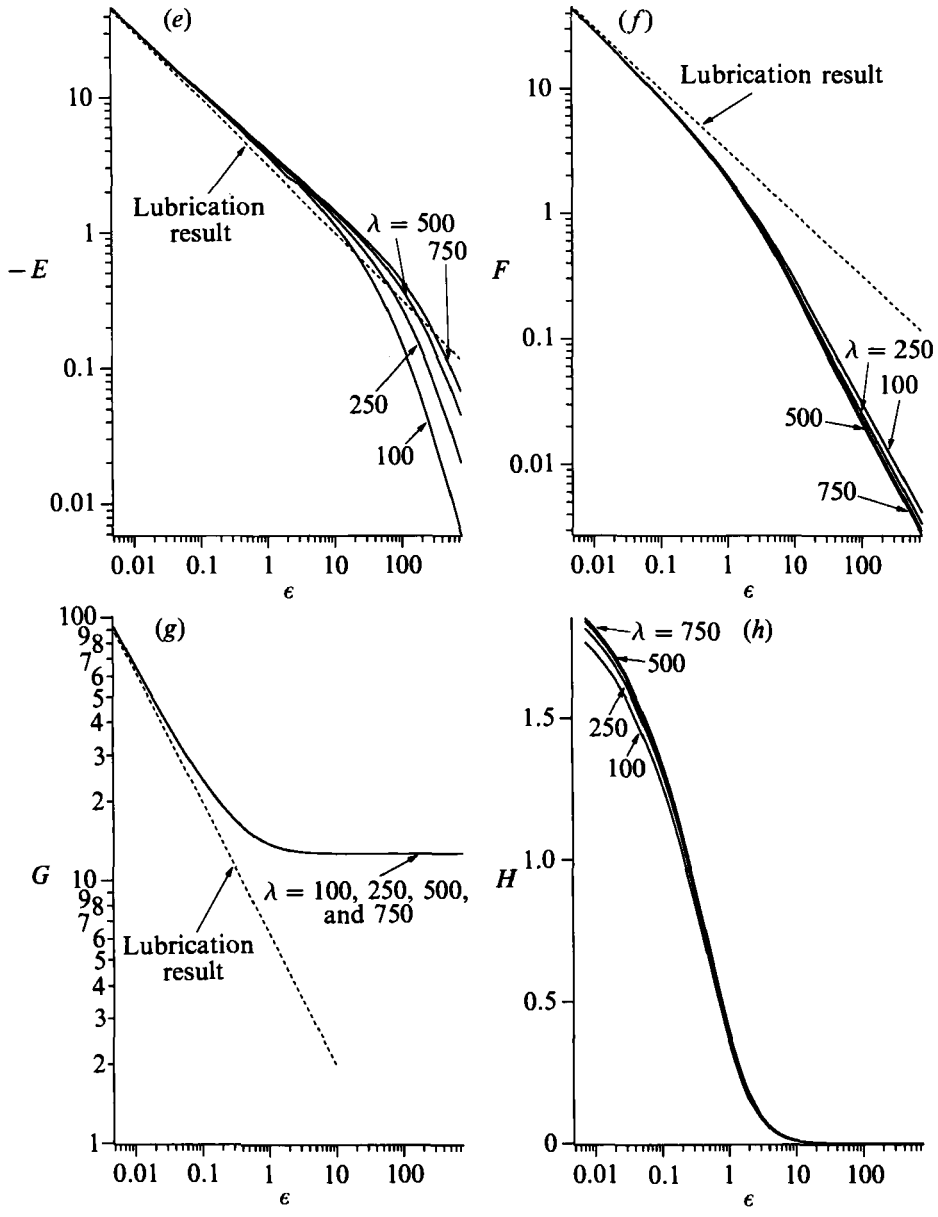

FIGURE 6. Elements of the resistivity matrix: (*a*)–(*h*) contain the resistivity functions *A*–*H*, respectively. In several of these graphs, minor discontinuities appear for $\lambda = 100$ when switching between the near-field solution and the uniformly valid approximation at $\epsilon = 2.0$.

We use the uniformly valid approximation for $\boldsymbol{M}$ for $\epsilon > 2$ and the inner solution for $\epsilon \leqslant 2.0$. For small values of ϵ, large values for the components of $\boldsymbol{R}$ are produced by small differences between components of $\boldsymbol{M}$ (see, for instance, the equations for A and B in Appendix A). The accuracy of this conversion is better using the near-field solution than the uniformly valid approximation. All scalars, except H, figure 6(*h*), have lubrication terms which dominate the results when $\epsilon \ll 1$. The lubrication terms are $O(\epsilon^{-\frac{3}{2}})$ for cases involving a squeezing motion and $O(\epsilon^{-\frac{1}{2}})$ for cases involving a shearing motion.

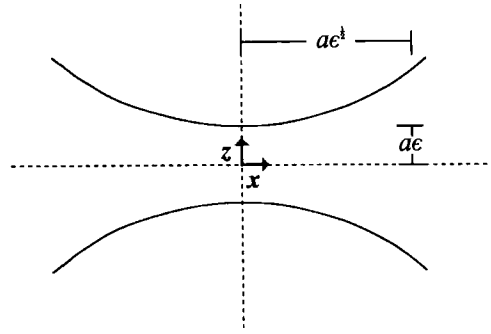

FIGURE 7. Schematic detailing the coordinate system for the calculation of the lubrication results.

The determination of the lubrication terms is analogous to the same problems for two spheres (Kim & Karrila 1991). The geometry is sketched in figure 7. For squeezing motion, the correct length and velocity scalings are $z = a\epsilon\bar{z}$, $x = a\epsilon^{\frac{1}{2}}\bar{x}$, and $u_z = U\bar{u}_z$, where each cylinder has equal and opposite velocity U. We formulate the lubrication problem in this way to ensure zero net force in the problem. This guarantees that the pressure and velocity fields decay. We are able to calculate components A and B of the resistivity matrix from these results by adding equal velocities to the two particles to make one particle stationary. The additional force introduced by this translation is small, $O(1)$, and does not affect the calculated forces. Thus, we only need to impose the correct relative velocity between the two particles. Continuing with the scaling, $u_x = U\epsilon^{-\frac{1}{2}}\bar{u}_x$ from continuity. Balancing the pressure with the leading-order term in the x-momentum equation gives $p = \epsilon^{-2}\mu U\bar{p}/a$. The leading-order results for the velocity and pressure fields are

$$\bar{u}_x = \tfrac{1}{2}(\partial\bar{p}/\partial x)\,[z^2 - (1+\tfrac{1}{2}x^2)^2] \tag{27}$$

and

$$\bar{p} = \tfrac{3}{2}(1+\tfrac{1}{2}x^2\}^{-2}. \tag{28}$$

The force for the cylinders differs from the sphere case because $F = h\int p\,\mathrm{d}x$ instead of $2\pi\int pr\,\mathrm{d}r$. Since $\mathrm{d}x \approx \epsilon^{\frac{1}{2}}$, $F \approx p \times \text{area} \approx O(\epsilon^{-\frac{3}{2}})$ for the cylinder instead of $O(\epsilon^{-1})$ for the sphere.

For shearing motion, we again have $z = a\epsilon\bar{z}$ and $x = a\epsilon^{\frac{1}{2}}\bar{x}$. Now, however, $u_x = V\bar{u}_x$, where V equals U or ωa. Again, in order to avoid non-decaying solutions, we formulate the lubrication problems with zero net force. Thus, the translational problem, $V = U$, is solved with equal and opposite velocities on the two particles. From continuity, $u_z = V\epsilon^{\frac{1}{2}}\bar{u}_z$, and from the x-momentum equation, $p = \epsilon^{-\frac{3}{2}}\mu V\bar{p}/a$. For this case, the leading-order results for the velocity and pressure fields are

$$\bar{u}_x = \frac{1}{2}\frac{\partial\bar{p}}{\partial\bar{x}}[\bar{z}^2 - (1+\tfrac{1}{2}\bar{x}^2)^2] + \frac{1}{2}\left[\frac{\bar{z}(U^{(1)} + a\omega^{(1)} - U^{(2)} + a\omega^{(2)})}{1+\tfrac{1}{2}\bar{x}^2} + U^{(1)} + a\omega^{(1)} + U^{(2)} - a\omega^{(2)}\right] \tag{29}$$

and

$$\bar{p} = \frac{(U^{(1)} + U^{(2)} - c)\,\bar{x}}{V(\bar{x}^2+2)^2} + \frac{1}{V}[\tfrac{3}{4}(U^{(1)} + U^{(2)} - c) + (a\omega^{(1)} - a\omega^{(2)})]\left[\frac{\bar{x}}{\bar{x}^2+2} + \frac{1}{\sqrt{2}}\tan^{-1}\frac{\bar{x}}{\sqrt{2}}\right], \tag{30}$$

where the value of c is determined by the boundary condition $\bar{p} \to 0$ as $\bar{x} \to \infty$. The force for the cylinders is $F = h\mu\int(\partial u_x/\partial z)\,\mathrm{d}x$, compared to $\mu\int(\partial u_x/\partial z)\,\mathrm{d}r$ for spheres.

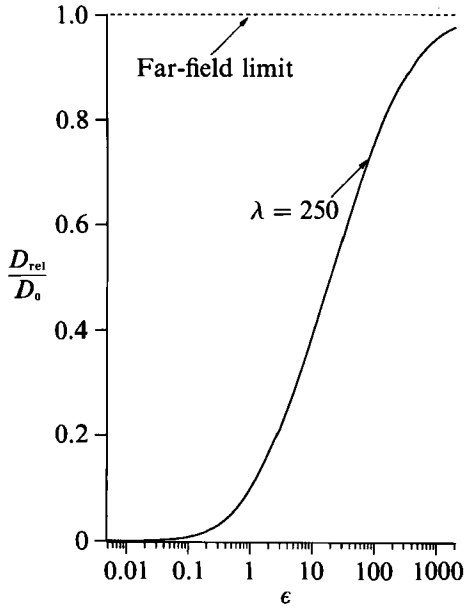

FIGURE 8. The normalized relative diffusivity, D_{rel}/D_0, between two cylinders as a function of gap width.

Component	Lubrication result
A	$\frac{3}{2}\pi\epsilon^{-\frac{3}{2}}$
B	$-\frac{3}{2}\pi\epsilon^{-\frac{3}{2}}$
C	$\pi\epsilon^{-\frac{1}{2}}$
D	$\pi\epsilon^{-\frac{1}{2}}$
E	$-\pi\epsilon^{-\frac{1}{2}}$
F	$\pi\epsilon^{-\frac{1}{2}}$
G	$2\pi\epsilon^{-\frac{1}{2}}$
H	$O(1)$

TABLE 1. The lubrication results for the components of $\boldsymbol{R}$

Therefore, as in the case of squeezing motion, the differing area gives larger shear forces in the cylinder case, $F \approx O(\epsilon^{-\frac{1}{2}})$, than in the sphere case. As mentioned earlier, H is independent of any lubrication contributions. This occurs because the torque generated by the force in the z-direction exactly cancels the torque generated by the force in the x-direction. This contrasts with the result for the analogous resistivity coefficient for spheres which has an $O(\ln\epsilon)$ singularity (Kim & Karrila 1991). The leading-order results for the components of $\boldsymbol{R}$ resulting from the lubrication analyses are given in table 1.

A key application of the mobility results is the calculation of the various diffusion tensors for a system of two proteins. For example, the relative translational diffusivity for two proteins along their line of centres is given by

$$D_{rel} = \frac{2(a-b)\,k_b\,T}{\mu h}, \tag{31}$$

where k_b is Boltzmann's constant and T is the absolute temperature. Figure 8 is the

graph of D_{rel}/D_0 for $\lambda = 250$, where D_0 is the relative diffusivity between two proteins at infinite separation distance. The values for D_{rel} are applicable to the calculation of reaction–diffusion problems without any preferred orientation of reaction. Furthermore, every diffusion coefficient for the two-protein system is directly proportional to combinations of the coefficients appearing in the mobility matrix.

4. Discussion

We have calculated the mobility and resistivity matrices for the motion of two equal-sized cylinders moving through a thin viscous sheet surrounded by lower-viscosity fluid. We have shown that the numerical results agree with the analytical results in the lubrication and far-field regimes.

For instance, looking at figure 5(*b*), we see that the hydrodynamic interactions are long range, operating on a lengthscale of $O(\lambda)$ or $O(100)$ for protein–membrane systems. This same lengthscale dictates the distances at which D_{rel}, figure 8, differs significantly from the far-field result, D_0. This is extremely long range compared to other important protein–protein interactions. For example, the range of potential energy interactions is typically $O(1)$ (Abney *et al.* 1989).

The results that we have obtained strongly suggest that hydrodynamic interactions have a significant influence on motions and encounters between cylinders (proteins) constrained to a thin viscous film (membrane) between less viscous (aqueous) layers. These hydrodynamic interactions might help explain the discrepancies between experimental and theoretical values for the diffusion coefficients of integral membrane proteins at high protein concentrations (Saxton 1987). We are in the process of using the two-particle hydrodynamic interaction results to calculate diffusion coefficients for proteins in membrane suspensions in a manner analogous to the work of Batchelor (1983) and Russel & Gast (1986) for suspensions of spheres. We will then compare these results to the corresponding experimental data. Furthermore, these results have important implications for the calculation of diffusion-limited reaction rates between membrane-bound proteins. Because hydrodynamic interactions decrease the relative diffusivity between proteins even at low protein concentration, diffusion-limited reaction rates calculated with hydrodynamic interactions will be lower than those calculated ignoring them. It is possible that reactions previously considered as kinetically controlled, a conclusion reached with collision rates calculated without incorporation of hydrodynamic interactions, might actually be diffusion controlled.

It is worth noting that the results that we obtained in the lubrication regime probably are not universally applicable to all protein–membrane systems. Our near-field results are based on the assumptions of a continuum fluid between two rigid proteins and that the globular domains of the proteins can be ignored. One or both of these assumptions might break down as the gap width between the two proteins becomes small. In this regime, the globular domains of the proteins could significantly affect the protein interactions if their characteristic radius is larger than a, the radius of the cylindrical core. Even if the radius of the globular domains is smaller than a, and their effect on the hydrodynamic interactions is negligible, the rigid-body and continuum assumptions eventually break down. Proteins are likely to deform somewhat under the large lubrication forces generated as $\epsilon \to 0$. This deformation could significantly alter the interactions between the proteins. Rigorous treatment of the hydrodynamic interactions between deformable cylindrical particles would require constitutive relations relating the deformation to the applied forces. Also, the

continuum model is probably not valid at the short distances at which lubrication begins to dominate. The radius of the lipid molecules making up the fluid can be as large as $\frac{1}{4}$ the radius of the protein molecules for lipid molecules with a radius of 5 Å. Theoretical (Bitsanis *et al.* 1990) and experimental (Israelachvili & McGuiggan 1988) studies indicate that the apparent viscous resistance of a three-dimensional fluid grows when the separation is comparable to the molecular diameter of the liquid. It would be interesting to pursue similar studies to determine the viscous resistance between deformable cylinders (proteins) when their gap width is comparable to the molecular scale of the individual liquid (lipid) molecules. The continuum lubrication results for rigid bodies, however, provide a reference state from which to compare deformation and non-continuum effects.

We would like to thank A. S. Sangani for discussions concerning the twin-pole expansion technique. This work was supported by the National Science Foundation in the form of a Creativity Award (EID-8710373) to S. J. Bussell and a Presidential Young Investigator Award (BCS-8958632) to D. A. Hammer.

Appendix A

The relationships between the components of $\boldsymbol{R}$ and $\boldsymbol{M}$ are symmetric because both matrices have identical forms. We will write the relationships to convert $\boldsymbol{R}$ to $\boldsymbol{M}$, but the reverse operators are obtained by simply switching the case of every label. The relationships are

$$a = -A/(B^2-A^2), \quad b = B/(B^2-A^2), \tag{A 1a, b}$$

$$J = [(E^2-C^2)(H^2-G^2)+2(EH-CG)(F^2+D^2)+4DF(CH-EG)+(F^2-D^2)^2], \tag{A 1c}$$

$$c = \frac{-[C(H^2-G^2)-2DFH+G(F^2+D^2)]}{J}, \quad d = \frac{H(CF+DE)-G(EF+CD)-DF^2+D^3}{J}, \tag{A 1d, e}$$

$$e = \frac{E(H^2-G^2)-2DFG+H(F^2+D^2)}{J}, \quad f = \frac{H(EF+DC)-G(CF+ED)-FD^2+F^3}{J}, \tag{A 1f, g}$$

$$g = \frac{-[G(E^2-C^2)+2DFE+C(F^2+D^2)]}{J}, \quad h = \frac{H(E^2-C^2)+2DFC+E(F^2+D^2)}{J}, \tag{A 1h, i}$$

where J is an intermediate.

Appendix B

The derivatives of G_1 are given in terms of the derivatives of $\ln(r)$, and those for G_2 are given in terms of the derivatives of $r^2\ln(r)$. In the formulae, $r^2 = x_1^2+x_2^2$ and $n = p+q$.

Derivatives of G_1: when q is even

$$\left(\frac{\partial}{\partial x_1}\right)^p\left(\frac{\partial}{\partial x_2}\right)^q(\ln(r)) = (-1)^{(p+\frac{1}{2}q-1)}(n-1)!\,r^{(-n)}\cos n\theta, \tag{B 1}$$

and when q is odd

$$\left(\frac{\partial}{\partial x_1}\right)^p\left(\frac{\partial}{\partial x_2}\right)^q(\ln(r)) = (-1)^{(p+\frac{3}{2}(q-1))}(n-1)!\,r^{(-n)}\sin n\theta. \tag{B 2}$$

Derivatives of G_2: for $n < 2$

$$\left.\begin{aligned}
&\frac{\partial}{\partial x_1}(r^2\ln(r)) = 2r(\ln(r)+1)\cos\theta, \quad \frac{\partial}{\partial x_2}(r^2\ln(r)) = 2r(\ln(r)+1)\sin\theta,\\
&\left(\frac{\partial}{\partial x_1}\right)^2(r^2\ln(r)) = 2(\ln(r)+1)+\cos 2\theta, \quad \left(\frac{\partial}{\partial x_2}\right)^2(r^2\ln(r))\\
&\qquad\qquad = 2(\ln(r)+1)-\cos 2\theta,\\
&\left(\frac{\partial}{\partial x_1}\right)\left(\frac{\partial}{\partial x_2}\right)(r^2\ln(r)) = \sin 2\theta;
\end{aligned}\right\} \tag{B 3}$$

for $n \geqslant 2$ and q even

$$\left(\frac{\partial}{\partial x_1}\right)^p\left(\frac{\partial}{\partial x_2}\right)^q(r^2\ln(r)) = (-1)^{(n+q/2)}(n-2)!\,r^{(2-n)}\left[\cos n\theta+\frac{2q-n}{(n-2)}\cos[(n-2)\theta]\right]; \tag{B 4}$$

and for $n \geqslant 2$ and q odd

$$\left(\frac{\partial}{\partial x_1}\right)^p\left(\frac{\partial}{\partial x_2}\right)^q(r^2\ln(r)) = (-1)^{(n+\frac{1}{2}(q-1))}(n-2)!\,r^{(2-n)}\left[\sin n\theta+\frac{q-p}{(n-2)}\sin[(n-2)\theta]\right]. \tag{B 5}$$

Appendix C

The following theorem was taken from Sangani & Yao (1988).

THEOREM. *Let $\boldsymbol{u}_r$ be a function satisfying $\nabla^4\boldsymbol{u}_r = 0$ and be non-singular for $\boldsymbol{r}$ inside a circle at $\boldsymbol{r}^{(n)}$. Then,*

$$\frac{1}{2\pi}\int_0^{2\pi}\boldsymbol{u}_r(\boldsymbol{r})\cos l\theta\,\mathrm{d}\theta = \tfrac{1}{2}(1+\delta_{10})\frac{a^l}{l!}\left[\left(\frac{\partial}{\partial x_1}\right)^l-\frac{l}{4}\left(\frac{\partial}{\partial x_1}\right)^{l-2}\nabla^2+\frac{a^2}{4(1+l)}\left(\frac{\partial}{\partial x_1}\right)^l\nabla^2\right]\boldsymbol{u}_r(\boldsymbol{r}^{(n)}), \tag{C 1}$$

and

$$\frac{1}{2\pi}\int_0^{2\pi}\boldsymbol{u}_r(\boldsymbol{r})\sin l\theta\,\mathrm{d}\theta = \frac{1}{2}\frac{a^l}{l!}\left[\left(\frac{\partial}{\partial x_1}\right)^{l-1}\left(\frac{\partial}{\partial x_2}\right)-\frac{l-2}{4}\left(\frac{\partial}{\partial x_1}\right)^{l-3}\left(\frac{\partial}{\partial x_2}\right)\nabla^2 + \frac{a^2}{4(1+l)}\left(\frac{\partial}{\partial x_1}\right)^{l-1}\left(\frac{\partial}{\partial x_2}\right)\nabla^2\right]\boldsymbol{u}_r(\boldsymbol{r}^{(n)}) \tag{C 2}$$

where a is the radius of the circle. In (C 1) and (C 2), the terms with a negative order of differentiation with respect to x_1 must be set equal to zero. The integration is assumed to be along the circumference, i.e. for $|\boldsymbol{r}-\boldsymbol{R}^{(n)}| = a$.

REFERENCES

ABNEY, J. R., SCALETTAR, B. A. & OWICKI, J. C. 1989 Self diffusion of interacting membrane proteins. *Biophys. J.* **55**, 817–833.

BATCHELOR, G. K. 1983 Diffusion in a dilute polydisperse system of interacting spheres. *J. Fluid Mech.* **131**, 155–175.

BITSANIS, I., SOMERS, S. A., DAVIS, H. T. & TIRRELL, M. 1990 Microscopic dynamics of flow in molecularly narrow pores. *J. Chem. Phys.* **93**, 3427–3431.

BRADY, J. F. & BOSSIS, G. 1988 Stokesian dynamics. *Ann. Rev. Fluid Mech.* **20**, 111–157.

BRENNER, H. & O'NEILL, M. E. 1972 On the Stokes resistance of multiparticle systems in a linear shear field. *Chem. Engng Sci.* **27**, 1421–1439.

BUSSELL, S. J. 1992 Diffusion-limited reaction rates of integral membrane proteins. Ph.D. thesis, Cornell University.

HUGHES, B. D., PAILTHORPE, B. A. & WHITE, L. R. 1981 The translational and rotational drag on a cylinder moving in a membrane. *J. Fluid Mech.* **110**, 349–372.

ISRAELACHVILI, J. N. & MCGUIGGAN, P. M. 1988 Forces between surfaces in liquids. *Science* **241**, 795–800.

KIM, S. & KARRILA, S. J. 1991 *Microhydrodynamics: Principles and Selected Applications.* Butterworth-Heinemann.

LORENTZ, H. A. 1907 Ein allgemeiner Satz, die Bewegung einer reibenden Flussigkeit betreffend, nebst einigen Anwendungen desselben (A general theorem concerning the motion of a viscous fluid and a few applications from it). *Abh. Theoret. Phys.* **1**, 23–42.

PETERS, R. & CHERRY, R. J. 1982 Lateral and rotational diffusion of bacteriorhodopsin in lipid bilayers: experimental test of the Saffman–Delbruck equations. *Proc. Natl Acad. Sci. USA* **79**, 4317–4321.

PINK, D. A., LAIDLAW, D. J. & CHILSHOLM, D. M. 1986 Protein lateral movement in lipid bilayers: Monte Carlo simulation studies of its dependence upon attractive protein–protein interactions. *Biochim. Biophys. Acta* **863**, 9–17.

RUSSEL, W. B. & GAST, A. P. 1986 Nonequilibrium statistical mechanics of concentrated colloidal dispersions: hard spheres in weak flows. *J. Chem. Phys.* **84**, 1815–1826.

SAFFMAN, P. G. 1976 Brownian motion in thin sheets of viscous fluid. *J. Fluid Mech.* **73**, 593–602.

SAFFMAN, P. G. & DELBRUCK, M. 1975 Brownian motion in biological membranes. *Proc. Natl Acad. Sci. USA* **72**, 3111–3113.

SANGANI, A. S. & YAO, C. 1988 Transport processes in random arrays of cylinders. II. Viscous flow. *Phys. Fluids* **31**, 2435–2444.

SAXTON, M. J. 1987 Lateral diffusion in an archipelago: the effect of mobile obstacles. *Biophys. J.* **52**, 989–997.

SCHULZ, G. E. & SCHIRMER, R. H. 1979 Principles of Protein Structure. Springer.

VAZ, W. L. C., GOODSAID-ZALDUONDO, F. & JACOBSON, K. 1984 Lateral diffusion of lipids and proteins in bilayer membranes. *FEBS Lett.* **174**, 199–207.